

# Self-Assembly and Optical Property of Triblock Copolymers Made of Polystyrene and Oligo(*p*-phenyleneethynylene) in Different Mixtures of Toluene and Hexane

Hong Huo,<sup>†</sup> Kun Li,<sup>§</sup> Qing Wang,<sup>\*,§</sup> and Chi Wu<sup>\*,†,‡</sup>

Department of Chemistry, The Chinese University of Hong Kong, Shatin, N. T. Hong Kong; The Hefei National Laboratory for Physical Sciences at Microscale, Department of Chemical Physics, University of Science and Technology of China, Hefei, Anhui 230026, China; and Department of Materials Science and Engineering, The Pennsylvania State University, University Park, Pennsylvania 16802

Received June 5, 2007; Revised Manuscript Received July 6, 2007

**ABSTRACT:** Using a combination of laser light scattering (LLS), UV–vis, and fluorescence spectrometry methods, we comparatively examined the self-assembly and optical property of two triblock copolymers made of polystyrene (PS, coillike) and oligo(*p*-phenyleneethynylene) (OPE, rodlike) in different mixtures of toluene and hexane. For the coil–rod–coil (PS–OPE–PS) triblock copolymer, intrachain wrapping of the two soluble PS coil blocks on the insoluble middle OPE rod block in the solvent mixture reduces the  $\pi$ – $\pi$  stacking of OPE and makes it more planar, resulting in a red shift in its UV–vis and fluorescence spectra, presumably, due to the J-type aggregation. While for the rod–coil–rod (OPE–PS–OPE) triblock copolymer, two intrachain stacked insoluble OPE blocks are wrapped and stabilized by the soluble middle PS block in toluene. The addition of hexane, a nonsolvent of PS, leads to further interchain aggregation of OPE, resulting in large polymeric micelles with an insoluble OPE core and a soluble PS shell. The blue shift in its UV–vis and fluorescence spectra reflects that intrachain stacking and interchain packing of OPE in the core are mainly H-type; i.e., they are parallel to each other, which increases the  $\pi$ – $\pi$  interaction of OPE.

## Introduction

Block copolymers made of two flexible (coil) blocks can self-assemble into a range of microphase-separated supramolecular structures.<sup>1–3</sup> The self-assembly of block copolymers made of one coillike block and one rodlike block is also theoretically and experimentally studied, leading to a number of novel morphological structures with some tunable optical and electronic properties.<sup>4–17</sup> It is not surprising that the difference in the chain rigidity affects how they are packed during the self-assembly as well as their final supramolecular structures. Polymer chains with a conjugated rodlike backbone have some unique physical properties due to their delocalized  $\pi$ -electron structures.<sup>18–22</sup> The electronic and optical properties of conjugated polymers strongly depend on intermolecular interactions, i.e., how they are packed together. Phenyleneethynylene polymers (PPE) and oligomers (OPE) with  $\pi$ – $\pi^*$  transition induced higher chiroptical activities are one kind of conjugated molecule with a range of applications in displays, sensors, and molecular electronics.<sup>23–27</sup> The PPE-type molecules were first synthesized in 1983.<sup>28</sup>

In order to increase their solubility and processability, alkyl or alkoxy side chains are often introduced. Recently, incorporation of conjugated polymer blocks into a polymer chain has opened a new way to control the chain packing and adjust their electronic and optical properties. As expected, the self-assembly of A–B–A triblock copolymer chains is much more complicated than A–B diblock copolymer chains in a selective solvent. Up to now, only a limited number of studies of the

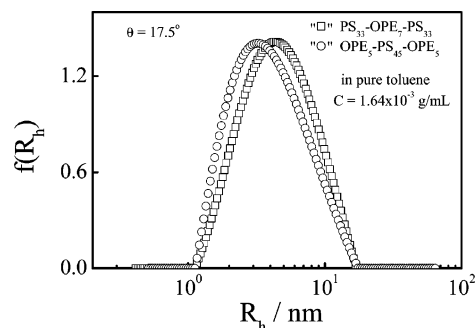


**Figure 1.** Hydrodynamic radius distributions of triblock copolymers (PS<sub>33</sub>–OPE<sub>7</sub>–PS<sub>33</sub> and OPE<sub>5</sub>–PS<sub>45</sub>–OPE<sub>5</sub>) chains in pure toluene.

self-assembly of triblock copolymers with one or two  $\pi$ -conjugated blocks have been reported.<sup>29–33</sup> Most of them were focused on their morphology in bulk. Less attention has been paid to how they are self-assembled in a selective solvent.<sup>34</sup> This is why we initiated the current study.

Using a combination of laser light scattering, UV–vis, and fluorescence spectroscopies, we comparatively studied the self-assembly and optical properties of one coil–rod–coil triblock copolymer and one rod–coil–rod triblock copolymer in different solvent mixtures of toluene and hexane, where the coil and rod blocks are polystyrene and oligo(*p*-phenyleneethynylene), respectively. The self-assembly occurs because the coil and rod blocks has a large difference in the Flory–Huggins segment–segment interaction parameter ( $\chi$ ) in the solvent mixture. Different arrangements of the coil and rod blocks in the triblock copolymers lead to different packings in the self-assembled structure and different optical properties.

\* To whom correspondence should be addressed at the Chinese University of Hong Kong.

<sup>†</sup> The Chinese University of Hong Kong

<sup>‡</sup> University of Science and Technology of China.

<sup>§</sup> The Pennsylvania State University.

**Table 1. GPC and LLS Characterization of Triblock Coil-Rod-Coil (PS<sub>33</sub>-OPE<sub>7</sub>-PS<sub>33</sub>) and Rod-Coil-Rod (OPE<sub>5</sub>-PS<sub>45</sub>-OPE<sub>5</sub>) Copolymers, Respectively, in THF and Pure Toluene at 25 °C**

sample	$M_{n,theory}$ (g/mol)	$M_{n,GPC}$ (g/mol)	$(M_w/M_n)_{GPC}$	$M_{w,LLS}$ (g/mol)	$(M_w/M_n)_{LLS}$	$\langle R_h \rangle$ (nm)
PS <sub>33</sub> -OPE <sub>7</sub> -PS <sub>33</sub>	$7.6 \times 10^3$	$7.5 \times 10^3$	1.15	$1.7 \times 10^4$	1.51	4.2
OPE <sub>5</sub> -PS <sub>45</sub> -OPE <sub>5</sub>	$5.7 \times 10^3$	$6.1 \times 10^3$	1.14	$5.0 \times 10^3$	1.68	3.2

## Experimental Section

**Sample Preparation.** The PS<sub>33</sub>-OPE<sub>7</sub>-PS<sub>33</sub> and OPE<sub>5</sub>-PS<sub>45</sub>-OPE<sub>5</sub> triblock copolymers were prepared by the condensation coupling between the amino-terminated OPE block and the carboxyl-terminated PS block that was synthesized by anionic polymerization. The synthetic details can be found elsewhere.<sup>30–33</sup> Analytical grade solvents, toluene and hexane, from Labscan Asia Co were used as received. The triblock copolymers were first dissolved in toluene with a concentration of 1.64 mg/mL at room temperature. The solutions were clarified with a 0.45 μm nylon filter to remove large dust particles. Different amounts of dust-free hexane were added to the clarified copolymer solution. Such prepared solutions were kept at room temperature for at least 24 h before laser light scattering measurements to ensure that hexane was completely mixed with toluene. One month later, the measurements were repeated to check whether the measured self-assembly of the triblock copolymer chains in the solvent mixtures had truly reached a stable state.

**Laser Light Scattering.** A modified commercial light scattering spectrometer (ALV/SP-125) equipped with an ALV-5000 multitaup digital time correlator and a He-Ne laser (output power = 22 mW at  $\lambda_0 = 632$  nm) was used. In static LLS, we were able to obtain both the weight-average molar mass ( $M_w$ ) and the z-average root-mean-square radius of gyration ( $\langle R_g^2 \rangle^{1/2}$  or written as  $\langle R_g \rangle$ ) of scattering objects in a dilute solution from the scattering vector ( $q$ ) dependence of the excess absolute scattering intensity, known as the Rayleigh ratio  $R_{vv}(q)$

$$\frac{KC}{R_{vv}(q)} \approx \frac{1}{M_w} \left( 1 + \frac{1}{3} \langle R_g^2 \rangle q^2 \right) + 2A_2C \quad (1)$$

where  $K = 4\pi^2 n^2 (dn/dC)^2 / (N_A \lambda_0^4)$ ,  $q = (4\pi n / \lambda_0) \sin(\theta/2)$ , and  $N_A$ ,  $dn/dC$ ,  $n$ , and  $\lambda_0$  are the Avogadro number, the specific refractive index increment, the solvent refractive index, and the wavelength of the light in a vacuum, respectively. The extrapolation to  $C \rightarrow 0$  and  $q \rightarrow 0$  can lead to  $M_w$ . The plots of  $[KC/R_{vv}(q)]_{C \rightarrow 0}$  vs  $q^2$  and  $[KC/R_{vv}(q)]_{q \rightarrow 0}$  vs  $C$  lead to  $\langle R_g^2 \rangle$  and  $A_2$ , respectively. For small scattering objects, the Zimm plot on the basis of eq 1 is usually used, which incorporates the extrapolations of  $C \rightarrow 0$  and  $q \rightarrow 0$  in a single grid. For the rod-coil-rod triblock copolymer (OPE<sub>5</sub>-PS<sub>45</sub>-OPE<sub>5</sub>), large self-assembled structures are formed due to strong intermolecular interaction in some solution mixtures so that the Berry plot

$$\left( \frac{KC}{R_{vv}(q)} \right)^{0.5} = \left( \frac{1}{M_w} \right)^{0.5} \left( 1 + \frac{1}{6} q^2 R_g^2 \right) (1 + A_2 M_w C) \quad (2)$$

was used to determine  $M_w$  and  $R_g$ . It is helpful to note that it is problematic to use static LLS to characterize the absolute  $M_w$  of a copolymer or aggregates of copolymer chains because the preferential adsorption of solvent on different comonomers. In the current study, the situation is even worse because we have to use a mixed solvent of toluene and hexane for some LLS measurements. Each solvent has a potential preferential adsorption problem. The classic LLS characterization of a copolymer in at least three solvents with different refractive indexes is not feasible here. Therefore, the values of  $M_w$  and  $R_g$  measured in this study are apparent ones, which will not affect the determination of the average aggregation number ( $N_{agg}$ ) because it is the ratio of  $M_{w,aggregates} / M_{w,chain}$ . In dynamic LLS, the Laplace inversion of each measured intensity-intensity time correlation function  $[(G^{(2)}(q, \tau) - B)/B]$  of scattering objects in a dilute solution can lead to a line-width distribution ( $G(\Gamma)$ ), where  $B$  is the measured baseline. The CONTIN Laplace inversion program in the correlator was used. For a pure diffusive relaxation,

$\Gamma$  is related to the translational diffusive coefficient ( $D$ ) by  $D = (\Gamma/q^2)_{q \rightarrow 0, C \rightarrow 0}$  and further to the hydrodynamic radius ( $R_h$ ) by  $R_h = k_B T / (6\pi\eta D)$ , where  $k_B$ ,  $\eta$ , and  $T$  are the Boltzmann constant, the solvent viscosity, and the absolute temperature, respectively. Therefore,  $G(\Gamma)$  can be converted to a distribution of translational diffusion coefficient ( $G(D)$ ) or a hydrodynamic radius distribution ( $f(R_h)$ ). The details of the LLS instrumentation and theory can be found elsewhere.<sup>35,36</sup>

**UV-vis and Fluorescence Measurements.** The UV-vis absorption and fluorescence spectra were recorded with a Varian Cary 5G UV-vis-NIR spectrometer and a Hitachi F-4500 fluorescence spectrometer, respectively. The excitation wavelength used in the fluorescence measurement was 332 nm. It should be stated that in order to compare results from different methods we used the same copolymer concentration for LLS, UV-vis, and fluorescence measurements. Since LLS required a more concentrated solution, we had to use a 1 mm thin quartz cuvette instead of a normal 10 mm one in the UV-vis measurement. All the UV-vis and fluorescence measurements were done at 25 °C.

## Results and Discussion

First, we used both LLS and GPC to characterize PS<sub>33</sub>-OPE<sub>7</sub>-PS<sub>33</sub> and OPE<sub>5</sub>-PS<sub>45</sub>-OPE<sub>5</sub>, respectively, in pure toluene and THF. Their number- and weight-average molar masses ( $M_n$  and  $M_w$ ) and the polydispersity indexes ( $M_w/M_n$ ) are summarized in Table 1. Figure 1 shows hydrodynamic radius distributions ( $f(R_h)$ ) of PS<sub>33</sub>-OPE<sub>7</sub>-PS<sub>33</sub> and OPE<sub>5</sub>-PS<sub>45</sub>-OPE<sub>5</sub> in pure toluene. The intensity-average hydrodynamic radius ( $\langle R_h \rangle$ ) calculated from each  $f(R_h)$  is also summarized in Table 1. For PS<sub>33</sub>-OPE<sub>7</sub>-PS<sub>33</sub>,  $\langle R_h \rangle \sim 4$  nm and  $M_{w,LLS}$  is  $1.7 \times 10^4$  g/mol, nearly 2 times higher than  $M_{w,GPC}$ . Moreover,  $(M_w/M_n)_{LLS}$  is much higher than  $(M_w/M_n)_{GPC}$ . Note that toluene as a solvent is only good for PS but poor for OPE. The previous SANS measurement showed that on average five PS<sub>33</sub>-OPE<sub>7</sub>-PS<sub>33</sub> chains can self-assemble to form spherical micelles in toluene when the polymer concentration is 26 mg/mL,<sup>32</sup> 15 times higher than what we used in the current LLS study. The SANS study also showed that the insoluble OPE core has a diameter of 4.4 nm, similar to the fully extended length of one OPE block ( $\sim 4.7$  nm), and the radius of gyration ( $R_g$ ) of the PS corona is 1.2 nm.<sup>32</sup> The higher the  $M_w$ , the broader distribution (higher  $M_w/M_n$ ) and the larger  $\langle R_h \rangle$  indicate that some of PS<sub>33</sub>-OPE<sub>7</sub>-PS<sub>33</sub> chains are still associated with each other even the solution is much dilute in the current case.

For OPE<sub>5</sub>-PS<sub>45</sub>-OPE<sub>5</sub>,  $M_{w,LLS} = 5.0 \times 10^3$  g/mol, slightly lower than  $M_{w,GPC}$ ,  $\langle R_h \rangle \sim 3$  nm, and  $(M_w/M_n)_{LLS} = 1.68$ . The results suggest that OPE<sub>5</sub>-PS<sub>45</sub>-OPE<sub>5</sub> mainly exists as individual chains in pure toluene, presumably due to its longer PS block and shorter OPE blocks in comparison with PS<sub>33</sub>-OPE<sub>7</sub>-PS<sub>33</sub>. Likely, the two OPE end blocks in OPE<sub>5</sub>-PS<sub>45</sub>-OPE<sub>5</sub> undergo an intrachain association in a dilute solution and then wrapped and stabilized by the longer PS middle block so that the interchain association ( $\pi$ - $\pi$  stacking) is suppressed. Note that our current LLS results are different from some previous TEM results.<sup>33</sup> The TEM micrographs of OPE<sub>5</sub>-PS<sub>45</sub>-OPE<sub>5</sub> in toluene showed various large microstructures, varying from hollow vesicular to spherical micelles, depending on the initial OPE<sub>5</sub>-PS<sub>45</sub>-OPE<sub>5</sub> concentration. It is possible that these large structures were formed during the TEM sample preparation; namely, toluene was removed by evaporation at the ambient

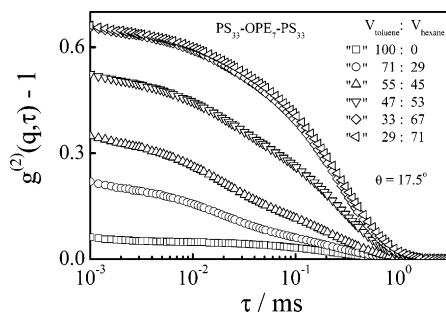


**Figure 2.** Typical normalized intensity-intensity time correlation functions of copolymer (PS<sub>33</sub>-OPE<sub>7</sub>-PS<sub>33</sub>) chains in different solvent mixtures of toluene and hexane.

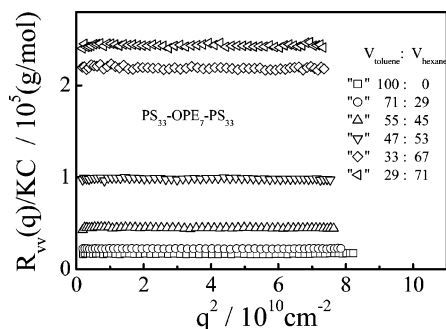


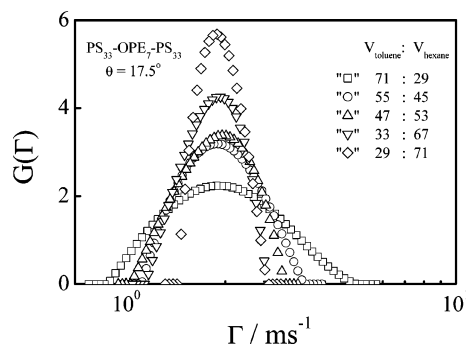
**Figure 3.** Scattering vector ( $q$ ) dependence of  $R_{vv}(q)/KC$  of copolymer (PS<sub>33</sub>-OPE<sub>7</sub>-PS<sub>33</sub>) chains in different solvent mixtures of toluene and hexane.

pressure and temperature, in which the copolymer concentration gradually increases.

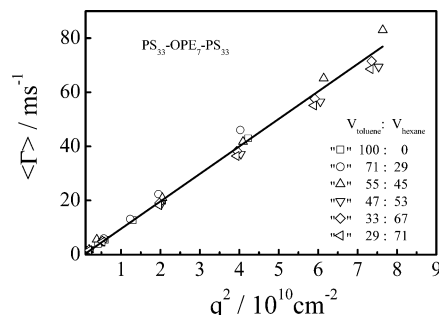
In order to enhance the interchain association, hexane as a nonsolvent for both the OPE and PS blocks was added. Figures 2 and 3 reveal that for PS<sub>33</sub>-OPE<sub>7</sub>-PS<sub>33</sub>, both the intercept of normalized time correlation function  $[(G^{(2)}(q, \tau) - B)/B]_{\tau \rightarrow 0}$ , i.e., the apparent coherence factor ( $\beta$ ), and the excess scattering intensity ( $R_{vv}(q)$ ) increase with the hexane content, but there is no significant change in the characteristic relaxation time, which can be better viewed in their corresponding line-width distributions from the Laplace inversion of  $(G^{(2)}(q, \tau) - B)/B$ , as shown in Figure 4. In Figure 3,  $[R_{vv}(q)/KC]_{q \rightarrow 0}$  leads to an apparent  $M_{w,LLS}$  because of a small concentration effect in the dilute regime and the previously discussed preferential adsorption problem. The results clearly show that interchain association is promoted after the addition of hexane. There is no angular dependence of  $R_{vv}(q)/KC$ , implying that most of the scattering objects in the solutions are fairly small in comparison with the wavelength of the laser light, or more precisely, with  $1/q$ . Each  $G(\Gamma)$  in Figure 4 leads to an average line width  $\langle \Gamma \rangle$  ( $\equiv \int_0^\infty G(\Gamma) \Gamma d\Gamma$ ).

Figure 5 shows that plots of  $\langle \Gamma \rangle$  vs  $q^2$  from PS<sub>33</sub>-OPE<sub>7</sub>-PS<sub>33</sub> in different mixtures of toluene and hexane collapse into a single straight line passing the origin, revealing that the relaxation measured in Figure 2 is purely diffusive. Moreover, it shows that the self-assembly or interchain association in different solvent mixtures leads to microstructures with a similar size ( $\langle R_h \rangle \sim 4$  nm). Table 2 summarizes effects of the hexane content on  $M_w$ , the average number of aggregation ( $N_{agg}$ ), and  $\langle R_h \rangle$ . When the hexane content is lower than 45%,  $M_w$  slightly increases with the hexane content and  $N_{agg}$  is less than 5. Further addition of hexane sharply increases  $M_w$  and finally leads to the precipitation when the hexane content is higher than  $\sim 71\%$ . The maximum measurable  $N_{agg}$  is about 28.

As expected, the soluble and swollen PS blocks in pure toluene can wrap and stabilize the insoluble OPE block. The



**Figure 4.** Characteristic line-width distributions of copolymer (PS<sub>33</sub>-OPE<sub>7</sub>-PS<sub>33</sub>) chains in different solvent mixtures of toluene and hexane.



**Figure 5.** Scattering vector ( $q$ ) dependence of average characteristic line-width ( $\langle \Gamma \rangle$ ) of copolymer (PS<sub>33</sub>-OPE<sub>7</sub>-PS<sub>33</sub>) chains in different solvent mixtures of toluene and hexane.

addition of hexane makes the PS blocks less soluble and shrunk so that interchain OPE association is promoted. It is helpful to note that the shrinking of the PS blocks decreases  $\langle R_h \rangle$ , but interchain association of OPE increases  $\langle R_h \rangle$ . This might explain why the average hydrodynamic radius ( $R_h$ ) of PS<sub>33</sub>-OPE<sub>7</sub>-PS<sub>33</sub> in different solvent mixtures remains a constant ( $\sim 4$  nm), close to the size of individual PS<sub>33</sub>-OPE<sub>7</sub>-PS<sub>33</sub> chains. The increase of  $M_w$  with the hexane content suggests that there exists equilibrium between individual chains and some self-assembled structures in the solvent mixture. With an increasing hexane content, the equilibrium shifts toward the self-assembly. The line width is narrowly distributed with a relative width of  $\sim 1.1$ – $1.2$ . The distribution becomes narrower when the hexane content increases, showing a gradual formation of well-defined aggregates. Note that the self-assembled structures are much more visible in light scattering, especially in dynamic LLS, because the scattering intensity ( $I$ ) is proportional to the square of the mass ( $M$ ) of scattering objects, i.e.,  $I \propto M^2$  and  $G(\Gamma)$  is a scattering intensity-weighted distribution.

How are the OPE blocks self-assembled in the solvent mixture? It has been known that the UV-vis absorption spectrum can reflect the status of the interchain  $\pi$ - $\pi$  stacking. Figure 6 shows several UV-vis absorption spectra of PS<sub>33</sub>-OPE<sub>7</sub>-PS<sub>33</sub> in different mixtures of toluene and hexane at the room temperature. When the hexane content is lower than 67%, there is only one broad peak in the absorption, located at 368 nm, typical for PS<sub>33</sub>-OPE<sub>7</sub>-PS<sub>33</sub> in toluene, but the peak slightly shifts to red as the hexane content increases. When the hexane content reaches 67%, the peak shifts to  $\sim 372$  nm and an additional peak appears at  $\sim 404$  nm. A comparison of LLS and UV-vis results shows that the equilibrium between individual chains and self-assembled structures significantly shifts toward to interchain association when the hexane content is higher than 67%. Clearly, LLS is more sensitive than UV-

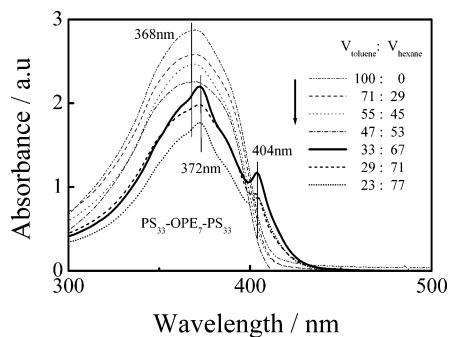


**Figure 6.** Typical UV-vis absorption spectra of copolymer (PS<sub>33</sub>-OPE<sub>7</sub>-PS<sub>33</sub>) chains in different solvent mixtures of toluene and hexane.

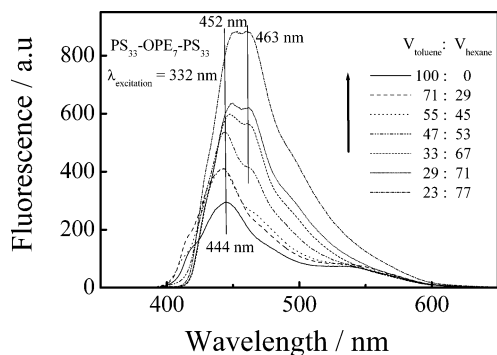


**Figure 7.** Typical fluorescence spectra of copolymer (PS<sub>33</sub>-OPE<sub>7</sub>-PS<sub>33</sub>) chains in different solvent mixtures of toluene and hexane.

vis because it can detect a trace amount of large interchain aggregates.

Figure 7 shows several fluorescence spectra of PS<sub>33</sub>-OPE<sub>7</sub>-PS<sub>33</sub> in different mixtures of toluene and hexane, where the excitation wavelength is 332 nm. In toluene, there are one peak at ~444 nm and one shoulder at ~547 nm. The addition of hexane shifts the peak from 444 to 452 nm and makes the shoulder disappear. Further addition of hexane leads to the emergence of another peak at 463 nm. The red shift and the second peak indicate the J-type  $\pi$ - $\pi$  interchain stacking. Figure 8 schematically shows the shift of the equilibrium from individual PS<sub>33</sub>-OPE<sub>7</sub>-PS<sub>33</sub> chains toward large self-assembled microstructures. The triblock copolymer mainly exists as individual chains in toluene because the insoluble OPE middle block is wrapped and stabilized by the two soluble PS end blocks. The addition of hexane reduces the solubility of PS so that the PS blocks collapse, resulting in interchain aggregation. The intrachain wrapping greatly reduces the interchain  $\pi$ - $\pi$  stacking of the OPE blocks and leads to the J-type aggregation. On the other hand, the intrachain wrapping also keeps the OPE backbone less bending so that it is in a more planar conformation.

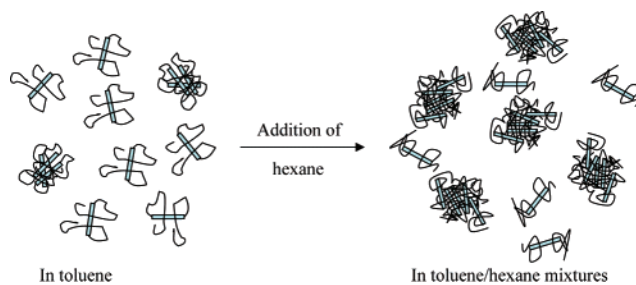


**Figure 8.** Schematic of shift of equilibrium between individual PS<sub>33</sub>-OPE<sub>7</sub>-PS<sub>33</sub> chains and self-assembled J-type aggregates as the hexane content increases.

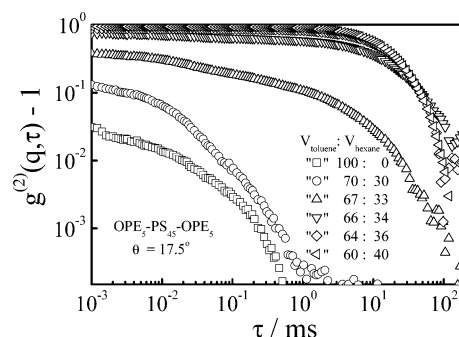


**Figure 9.** Typical normalized intensity-intensity time correlation functions of copolymer (OPE<sub>5</sub>-PS<sub>45</sub>-OPE<sub>5</sub>) chains in different solvent mixtures of toluene and hexane.

For OPE<sub>5</sub>-PS<sub>45</sub>-OPE<sub>5</sub>, its two end blocks become insoluble, while its middle block is now soluble. Figure 9 shows their typical intensity-intensity time correlation functions in different mixtures of toluene and hexane. Note that here the y-axis is in the logarithmical scale because OPE<sub>5</sub>-PS<sub>45</sub>-OPE<sub>5</sub> in pure toluene scatters little light in comparison with PS<sub>33</sub>-OPE<sub>7</sub>-PS<sub>33</sub> for a given concentration. The addition of hexane also increases the intercept of  $[(G^{(2)}(q, \tau) - B)/B]$  at  $\tau \rightarrow 0$ , just as in the case of PS<sub>33</sub>-OPE<sub>7</sub>-PS<sub>33</sub>. The dramatic change occurs in the hexane content range 30–36%. Such a change is better and directly reflected in the excess scattering intensity ( $\propto R_{vv}(q)$ ), as shown in Figure 10. On the basis of eqs 1 and 2, the extrapolation of  $KC/R_{vv}(q)$  at  $q \rightarrow 0$  and the slope of  $KC/R_{vv}(q)$  vs  $q^2$  lead to  $M_w$  and  $\langle R_g \rangle$ , respectively, which are summarized in Table 2.

Figure 11 shows two hydrodynamic radius distributions of OPE<sub>5</sub>-PS<sub>45</sub>-OPE<sub>5</sub> in pure toluene and in a toluene/hexane (60/40) mixture. When the hexane content is low, there is only one fast relaxation mode in  $G(\Gamma)$ . As the hexane content reaches 40%, another slow mode appears due to the formation of some large structures. At smaller scattering angles, the peak located at 0.3 ms gradually disappears as the hexane content increases, but it is still observable at large scattering angles, revealing the

**Table 2.** LLS Characterization of Triblock Coil-Rod-Coil (PS<sub>33</sub>-OPE<sub>7</sub>-PS<sub>33</sub>) and Rod-Coil-Rod (OPE<sub>5</sub>-PS<sub>45</sub>-OPE<sub>5</sub>) Copolymers in Different Mixtures of Toluene and Hexane at 25 °C

		PS <sub>33</sub> -OPE <sub>7</sub> -PS <sub>33</sub> (Coil-Rod-Coil)						
$V_{\text{toluene}}:V_{\text{hexane}}$	100:0	82:18	71:29	65:35	55:45	47:53	33:67	29:71
$M_w/10^4$ (g/mol)	1.7	1.7	2.2	3.4	4.5	9.9	22	24
$\langle R_h \rangle$ (nm)	4.2	4.1	4.2	4.3	4.3	4.7	4.6	4.6
$N_{\text{agg}}$	2	2	3	4	5	11	25	28
		OPE <sub>5</sub> -PS <sub>45</sub> -OPE <sub>5</sub> (Rod-Coil-Rod)						
$V_{\text{toluene}}:V_{\text{hexane}}$	100:0	94:6	78:22	70:30	67:33	66:34	64:36	60:40
$M_w/10^4$ (g/mol)	0.5	0.5	0.5	0.7	6.4	12	140	4600
$\langle R_g \rangle$ (nm)					106	152	199	226
$\langle R_h \rangle_{\text{fast}}$ (nm)	3.2	3.2	3.2	3.1	3.3	3.2	3.4	3.3
$\langle R_h \rangle_{\text{slow}}$ (nm)					366	374	381	385
$N_{\text{agg}}$	1.0	1.0	1.0	1.4	13	24	280	9200

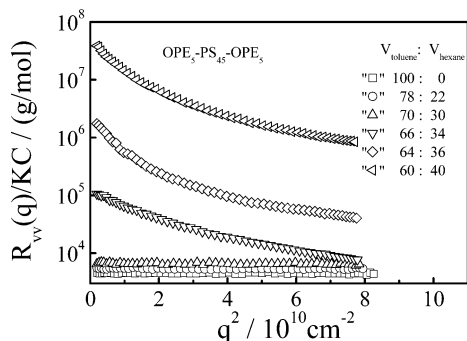


**Figure 10.** Scattering vector ( $q$ ) dependence of  $R_{v}(q)/KC$  of copolymer ( $OPE_5-PS_{45}-OPE_5$ ) chains in different solvent mixtures of toluene and hexane.

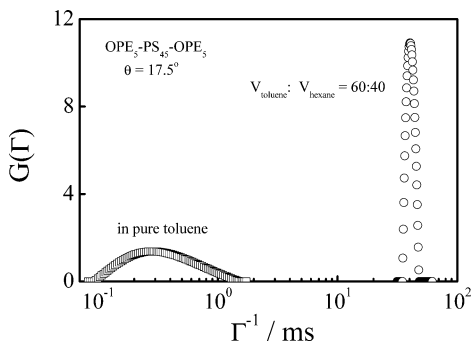


**Figure 11.** Characteristic line-width distributions of copolymer ( $OPE_5-PS_{45}-OPE_5$ ) chains in pure toluene and in different solvent mixture of toluene and hexane.

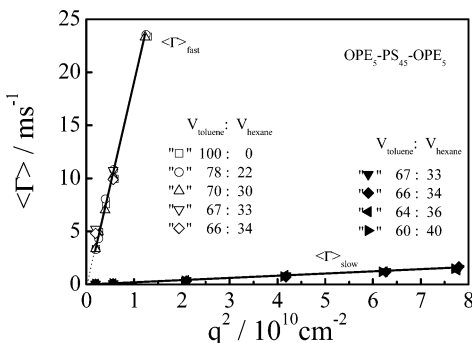


**Figure 12.** Scattering vector ( $q$ ) dependence of average characteristic line width ( $\langle\Gamma\rangle$ ) of copolymer ( $OPE_5-PS_{45}-OPE_5$ ) chains in different solvent mixtures of toluene and hexane.

coexistence of small individual chains and large self-assembled microstructures. The intensity contribution of such large aggregates at small scattering angles is so high that individual chains become “invisible” in LLS. For both of the peaks,  $\langle\Gamma\rangle$  is a linear function of  $q^2$  and the extrapolation at of  $\langle\Gamma\rangle$  vs  $q^2$  to  $q \rightarrow 0$  passes the origin, as shown in Figure 12, indicating that both the fast and slow modes are diffusive. The collapse of  $\langle\Gamma\rangle_{\text{fast}}$  vs  $q^2$  to a single line is expected because the fast mode is related to individual chains. Unexpected, plots of  $\langle\Gamma\rangle_{\text{slow}}$  vs  $q^2$  also collapse into a single straight line, revealing that large interchain aggregates have a similar size. The values of  $\langle R_h \rangle$  for both the fast and slow modes calculated from  $(\langle\Gamma\rangle/q^2)_{q \rightarrow 0}$  also listed in Table 2.

The values of  $M_w$  and  $\langle R_h \rangle$  of  $OPE_5-PS_{45}-OPE_5$  in pure toluene as well as in the mixtures with a small amount of hexane reveal that the solution mainly contains individual chains. Presumably, two insoluble shorter OPE end blocks undergo intrachain association and then wrapped and stabilized by the relatively longer soluble middle PS block. The addition of more

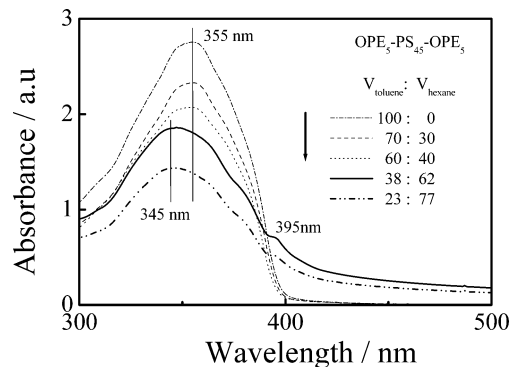


**Figure 13.** Typical UV-vis absorption spectra of copolymer ( $OPE_5-PS_{45}-OPE_5$ ) chains in different solvent mixtures of toluene and hexane.

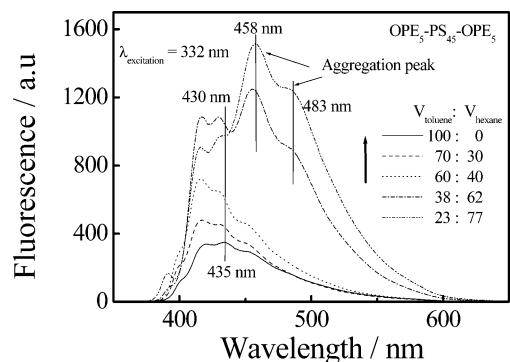


**Figure 14.** Typical fluorescence spectra of copolymer ( $OPE_5-PS_{45}-OPE_5$ ) chains in different solvent mixtures of toluene and hexane.

hexane makes the PS block less soluble so that interchain OPE association starts, resulting in large self-assembled structures. In the range 33–40%,  $\langle R_h \rangle_{\text{slow}}$  nearly remains a constant, but  $\langle R_g \rangle$  increases with the hexane content. Note that individual chains in the solvent mixture also scatter light and  $\langle R_g \rangle$  reflects an average of individual chains and large aggregates. As the hexane content increases, the equilibrium shifts toward the formation of more large aggregates so that  $\langle R_g \rangle$  increases.

Table 2 shows that  $\langle R_g \rangle / \langle R_h \rangle$  approaches 0.6 when the hexane content reaches  $\sim 40\%$ . It is known that for a flexible random coil chain in an athermal solvent,  $\langle R_g \rangle / \langle R_h \rangle \sim 1.5$ , and for a uniform hard sphere,  $\langle R_g \rangle / \langle R_h \rangle \sim 0.774$ . The lower values of  $\langle R_g \rangle / \langle R_h \rangle$  reflect that the center of large self-assembled structures has a higher density than the periphery. On the other hand, the scattering intensity ( $I$ ) is scaled to the scattering vector ( $q$ ) as  $I \propto q^{-2.5}$  when the hexane content reaches 40%, suggesting that the self-assembly is a reaction-limited process and the aggregates have a more compact structure since the wrapping of the middle PS block reduces the sticking probability. Our LLS results reveal that due to the structure difference of the two triblock copolymers,  $OPE_5-PS_{45}-OPE_5$  can form large self-assembled structures, but not  $PS_{33}-OPE_7-PS_{33}$ , in the same solvent mixtures.

Figure 13 shows that several absorption spectra of  $OPE_5-PS_{45}-OPE_5$  in different solvent mixtures. When the hexane content is low, the spectrum is insensitive to the addition of hexane. As the hexane content reaches  $\sim 62\%$ , the main peak slightly shifts to blue from 355 to 345 nm and another peak emerges at 395 nm, signaling the formation of large self-assembled microstructures. Previous studies also showed a similar blue shift after short unsubstituted oligothiophene or  $\alpha,\omega$ -substituted oligothiophene chains were placed in a Langmuir-Blodgett or vacuum-deposited thin film.<sup>33,37–39</sup> Such a blue shift has been attributed to a parallel alignment of the conjugated

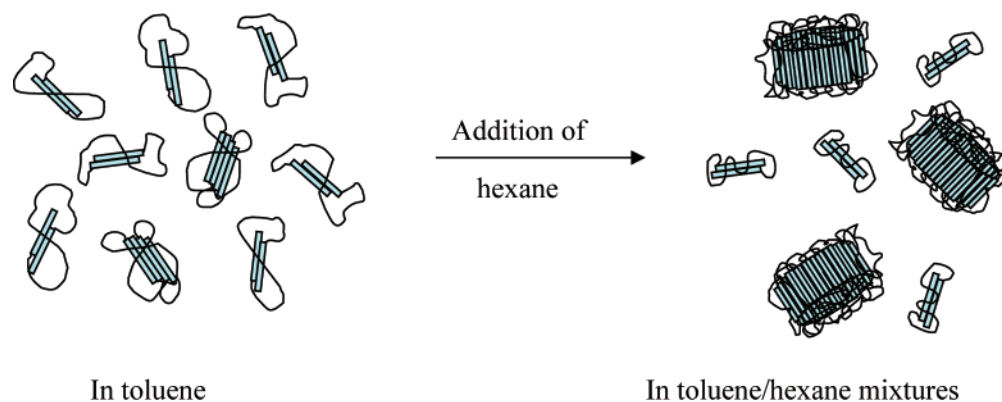


**Figure 15.** Schematic of shift of equilibrium between individual copolymer (OPE<sub>5</sub>-PS<sub>45</sub>-OPE<sub>5</sub>) chains and large self-assembled core-shell structures with a H-type OPE core as the hexane content increases.

OPE blocks along their long axes, i.e., the so-called H-type aggregation.

Further, Figure 14 shows that the fluorescence spectra of OPE<sub>5</sub>-PS<sub>45</sub>-OPE<sub>5</sub> in toluene has two peaks located at 415 and 435 nm plus one shoulder at 455 nm. The spectrum slightly shifts to blue when a small amount of hexane is added. Further addition of hexane to 62% leads to a dramatic change in the spectrum, fairly consistent with the UV-vis absorption results. The fluorescence study further confirms that the OPE blocks are aligned in a parallel fashion to form the H-type aggregates via the  $\pi$ - $\pi$  interaction. Note that some of previous studies of rod-coil-rod copolymer chains in a selective solvent showed the formation of spherical hollow vesicles,<sup>40-42</sup> different from the current core-shell micelle-like structures made of OPE<sub>5</sub>-PS<sub>45</sub>-OPE<sub>5</sub>. Such a structure difference is normal since the delicate balance between soluble and insoluble blocks can greatly affect their self-assembled microstructures. Figure 15 schematically shows the shift of the equilibrium between individual rod-coil-rod triblock copolymer OPE<sub>5</sub>-PS<sub>45</sub>-OPE<sub>5</sub> chains and their self-assembled structures after the addition of hexane.

## Conclusion

Different combinations of rodlike and coil-like blocks in a triblock copolymer, i.e., coil-rod-coil or rod-coil-rod, can affect its self-assembly and optical properties in a selective solvent. The studies of polystyrene-oligo(*p*-phenyleneethynylene)-polystyrene (PS<sub>33</sub>-OPE<sub>7</sub>-PS<sub>33</sub>) and oligo(*p*-phenyleneethynylene)-polystyrene-oligo(*p*-phenyleneethynylene) (OPE<sub>5</sub>-PS<sub>45</sub>-OPE<sub>5</sub>) in different solvent mixtures of toluene and hexane by a combination of laser light scattering, UV-vis, and fluorescence spectrometries reveal that (1) the self-assembled microstructure is strongly influenced by the copolymer structure even for a given solvent mixture; (2) in the solvent mixture, there exists an equilibrium between individual triblock copolymer chain and self-assembled micelle-like structures; and (3) the addition of hexane shifts the equilibrium to the self-assembly. For PS<sub>33</sub>-OPE<sub>7</sub>-PS<sub>33</sub>, the two coil-like PS end blocks can wrap the rodlike OPE middle block and make the conjugated OPE backbone more stiff and planar, but the intrachain wrapping prevents a parallel alignment of OPE and suppresses the  $\pi$ - $\pi$  interaction. For OPE<sub>5</sub>-PS<sub>45</sub>-OPE<sub>5</sub>, the two conjugated rodlike OPE end blocks can undergo a parallel intrachain association in the dilute solution to form the  $\pi$ - $\pi$  stacking and stabilized by the PS block. The addition of hexane can also induce interchain parallel association of OPE to form a disklike core stabilized by a soluble PS shell. The packing of the OPE blocks of the two triblock copolymers in the solution mixture results

in different optical properties. The J-type aggregation shifts the UV-vis and fluorescence spectra of PS<sub>33</sub>-OPE<sub>7</sub>-PS<sub>33</sub> to red, while the H-type aggregation shifts the UV-vis and fluorescence spectra of OPE<sub>5</sub>-PS<sub>45</sub>-OPE<sub>5</sub> to blue.

**Acknowledgment.** The financial support of the Chinese Academy of Sciences (CAS) Special Grant (KJCX2-SW-H14), the National Natural Scientific Foundation of China (NNSFC) Projects (20534020 and 20574065), and the Hong Kong Special Administration Region (HKSAR) Earmarked Project (CUHK4025/04P, 2160242) is gratefully acknowledged.

## References and Notes

- Helfand, E.; Wasserman, Z. R. *Macromolecules* **1980**, *13*, 994.
- Hashimoto, T.; Shibayama, M.; Kawai, H. *Macromolecules* **1983**, *16*, 1093.
- Leibler, L. *Macromolecules* **1980**, *13*, 1602.
- Zhang, L.; Eisenberg, A. *Science* **1995**, *268*, 1728.
- Jenekhe, S. A.; Chen, X. L. *Science* **1998**, *279*, 1903.
- Jenekhe, S. A.; Chen, X. L. *Science* **1999**, *283*, 372.
- Harada, A.; Kataoka, K. *Science* **1999**, *283*, 65.
- Won, Y. Y.; Dvis, H. T.; Bates, F. S. *Science* **1999**, *283*, 960.
- Discher, B. M.; Disher, D. E.; Hammer, D. A. *Science* **1999**, *284*, 1143.
- Tew, G. N.; Pralle, M. U.; Stupp, S. I. *Angew. Chem., Int. Ed.* **2000**, *39*, 517.
- Lee, M.; Cho B. K.; Zin W. C. *Chem. Rev.* **2001**, *101*, 3869.
- Schoonbeek, F. S.; Van, Esch, J. H.; Wegewijs, B.; Diederik, B. A. R.; Matthijs, P. H.; Klapwijk, T. M.; Kelloog, R. M.; Feringa, B. L. *Angew. Chem., Int. Ed.* **1999**, *38*, 1393.
- Wang, H. B.; You, W.; Jiang, P.; Yu, L. H.; Wang, H. *Chem.-Eur. J.* **2004**, *10*, 986.
- Sayar, M.; Stupp, S. I. *Macromolecules* **2001**, *34*, 7135.
- Halperin, A. *Macromolecules* **1990**, *23*, 2724.
- Tu, Y. F.; Wan, X. H.; Zhang, H. L.; Fan, X. H.; Chen, X. F.; Zhou, Q. F.; Chau, K. C. *Macromolecules* **2003**, *36*, 6565.
- Hoeben, F.; Jonkheijm, P.; Meijer, E.; Schenning, A. P. H. J. *Chem. Rev.* **2005**, *105*, 1491.
- Breitenkamp, R. B.; Tew, G. N. *Macromolecules* **2004**, *37*, 1163.
- Halkyard, C. E.; Rampey, M. E.; Kloppenburg, L.; Studer-Martinez, S. L.; Bunz, U. H. F. *Macromolecules* **1998**, *31*, 8655.
- Menon, A.; Galvin, M.; Walz, K. A.; Rothberg, L. *Synth. Met.* **2004**, *141*, 197.
- Zahn, S.; Swager, T. M. *Angew. Chem., Int. Ed.* **2002**, *41*, 4225.
- Egbe, D.; Tillmann, H.; Birkner, E.; Klemm, E. *Macromol. Chem. Phys.* **2001**, *202*, 2712.
- Fiesel, R.; Scherf, U. *Macromol. Rapid Commun.* **1998**, *19*, 427.
- Levitus, M.; Schmieder, K.; Ricks, H.; Shimizu, K. D.; Bunz, U. H. F.; Garcia-Garibay, M. A. *J. Am. Chem. Soc.* **2001**, *123*, 4259.
- Fan, Q. L.; Zhou, Y.; Lu, X. M.; Hou, X. Y.; Huang, W. *Macromolecules* **2005**, *38*, 2927.
- Breitenkamp, R. B.; Tew, G. N. *Macromolecules* **2004**, *37*, 1163.
- Chu, Q. H.; Pang, Y. *Macromolecules* **2003**, *36*, 4614.
- Lakmikantham, M. V.; Vartikar, J.; Kwan, Y. J.; Cava, M. P.; Huang, W. S.; MacDiarmid, A. *Polym. Prepr. (Am. Chem. Soc., Div. Polym. Chem.)* **1983**, *24*, 75.
- Mori, T.; Watanabe, T.; Minagawa, K.; Tanaka, M. *J. Polym. Sci., Part A: Polym. Chem.* **2005**, *43*, 1569.

- (30) Li, K.; Wang, Q. *Macromolecules* **2004**, *37*, 1172.
- (31) Li, K.; Guo, L.; Liang, Z. Q.; Thiyagarajan, P.; Wang, Q. *J. Polym. Sci., Part A: Polym. Chem.* **2005**, *43*, 6007.
- (32) Li, K.; Wang, Q. *Chem. Commun.* **2005**, 4786.
- (33) Cuendias, A.; Hellaye, M. L.; Lecommandoux, S.; Cloutet, E.; Cramail, H. *J. Mater. Chem.* **2005**, *15*, 3264.
- (34) Tu, Y. F.; Wan, X. H.; Zhang, D.; Zhou, Q. F.; Wu, C. *J. Am. Chem. Soc.* **2000**, *122*, 10201.
- (35) Ngai, T.; Wu, C. *Macromolecules* **2003**, *36*, 848.
- (36) Ngai, T.; Wu, C.; Chen, Y. *J. Phys. Chem. B* **2004**, *108*, 5532.
- (37) Hotta, S.; Waragi, K. *J. Phys. Chem.* **1993**, *97*, 7427.
- (38) Yassar, A.; Horowitz, G.; Valat, P.; Wintgens, V.; Hymene, M.; Deloffre, F.; Sirvastava, P.; Lang, P.; Garnier, F. *J. Phys. Chem.* **1993**, *97*, 7427.
- (39) Schoeler, U.; Tew, K. H.; Kuhn, H. *J. Chem. Phys.* **1974**, *61*, 5009.
- (40) Jenekhe, S. A.; X.; Chen, L. *J. Phys. Chem. B* **2000**, *104*, 6332.
- (41) Chen, X. L.; Jenekhe, S. A. *Macromolecules* **2000**, *33*, 4610.
- (42) Rahman, M. S.; Samal, S.; Lee, J. S. *Macromolecules* **2006**, *39*, 5009.

MA071247K